Check for updates

Palladium nanoparticles from β-cyclodextrin and cellulose methyl carboxylate as an effective catalyst for Sonogashira coupling and the reduction of alkynes†

Van-Dung Le, [ID] *[ab] T. Kim Chi Huynh, [ID] [ab] Van Nam Dao,[ab] Chi-Hien Dang[ab] and Thi Yen Nghi Le[ab]

This research presents an effective approach for synthesizing palladium nanoparticle (PdNP) catalysts, employing β-cyclodextrin (β-CD) as a reducing agent and cellulose methyl carboxylate (CMC) as a stabilizer. PdNP-based nanocomposites were prepared by varying the mass ratios of CMC to β-CD from 1:1 to 3:2. Their structural and physicochemical properties were thoroughly analyzed using multiple characterization techniques, including ultraviolet-visible spectroscopy (UV-vis), FTIR, DLS, Zeta potential, XRD, TGA, and TEM. The resulting PdNPs exhibited a crystalline structure with particle dimensions spanning from 2 to 10 nm, with the majority falling between 4 and 6 nm. These nanoparticles demonstrated outstanding catalytic activity in Sonogashira coupling reactions, operating without additional catalysts and efficiently converting alkynes into (Z)-alkenes utilizing KOH/DMF as a hydrogen donor. The high yield and selectivity observed highlight the potential of CMC/β-CD-stabilized PdNPs as promising catalysts for organic synthesis applications.

1. Introduction

Transition metal nanoparticles have a vital function in heterogeneous catalysis due to their extensive surface area, which provides numerous highly active, unsaturated metal sites.[1–3] Among these, palladium nanoparticles (PdNPs) have gained significant attention for their wide-ranging applications in biochemical research, pharmaceuticals, and organic synthesis.[4–8] The eco-friendly production of PdNPs utilizing organic materials like plant extracts, natural substances, and polysaccharides presents multiple benefits, such as affordability, straightforward synthesis, and outstanding biocompatibility.[9,10]

Palladium-catalyzed coupling reactions play a vital role in synthesizing complex organic molecules by facilitating carbon–carbon bond formation.[11–13] Employing palladium as a homogeneous catalyst has greatly improved the effectiveness of numerous cross-coupling reactions, including the Sonogashira, Heck, and Stille reactions.[14–19] Recent studies on PdNPs has focused on improving their catalytic activity and selectivity in

different transformations.[20–31] Notably, PdNPs have demonstrated high efficiency in the targeted hydrogenation of alkynes into (Z)-alkenes in DMF/KOH without requiring molecular hydrogen. Their ability to enhance reaction efficiency under milder and more sustainable conditions aligns with the principles of green chemistry. Moreover, PdNPs can facilitate cross-coupling reactions without the need for additional ligands or co-catalysts, further increasing their practical applicability.[32–42]

A previous study indicated that β-CD was also employed to cap palladium nanoparticles, using NaBH$_4$ as the reducing agent. This approach proved effective for the Sonogashira coupling reaction in water without the presence of CuI.[43] In this study, β-CD in a basic medium can reduce Pd^{2+} to PdNPs, while CMC serves as a good and inexpensive support but is difficult to separate from water by centrifugation. Moreover, if β-CD alone is used to reduce Pd^{2+} to Pd^0 without the presence of CMC, the palladium nanoparticles tend to aggregate very quickly. However, the combination of CMC and CD can form hydrogen interactions between glucose molecules, making it easier to centrifuge out of the aqueous solution, and the resulting palladium nanoparticles are more stable.

In addition, the catalytic efficiency has been demonstrated in the Sonogashira reaction with a maximum reaction time of 3 hours, and the yields of the purified products after column chromatography exceed 90%. In the revised manuscript, to further evaluate the catalyst's performance, we extended its application to the selective hydrogenation of alkynes to (Z)-

aInstitute of Chemical Technology, Vietnam Academy of Science and Technology, 1A, TL29 Street, Thanh Loc Ward, District 12, Ho Chi Minh City, Vietnam. E-mail: tohoahocctb@gmail.com

bGraduate University of Science and Technology, Vietnam Academy of Science and Technology, 18 Hoang Quoc Viet, Cau Giay, Hanoi, Vietnam

† Electronic supplementary information (ESI) available. See DOI: https://doi.org/10.1039/d4ra07789j

alkenes. The results showed isolated yields above 90%, with a predominant (*Z*)-alkene configuration. Currently, we are also employing these catalysts for other reactions, such as the Heck reaction and the reduction of nitrophenol. Initial results indicate excellent catalytic performance, with a short reaction time (approximately 4 hours) for the Heck reaction. Thus, this catalytic system holds great potential for organic synthesis.

2. Materials and methods

2.1. Materials

Aryl halides and alkynes were utilized in their original form without undergoing additional purification. The key reagents, including β-cyclodextrin (β-CD, 98%), carboxymethyl cellulose, sodium salt (CMC, M. W. = 250 000, DS = 1.2), and palladium(II) acetate (Pd(OAc)$_2$, 99.9%)were obtained from Acros (Belgium). The compounds 2-(hex-3-yn-1-yloxy)tetrahydro-2*H*-pyran and 2-(oct-3-yn-1-yloxy)tetrahydro-2*H*-pyran were synthesized according to a previously reported method.[44]

2.2. Preparation of gel β-CD-CMC

β-CD and CMC were blended at mass ratios of 1 : 1, 2 : 1, and 3 : 2 (w/w) and transferred into a 250 mL round-bottom flask. The mixture was then dispersed in 30 mL of water and subjected to sonication until a uniform solution was achieved. This procedure led to the formation of gel formulations labeled as β-CDCMC11, β-CDCMC12, and β-CDCMC32. The resulting gels were later freeze-dried and kept at room temperature for future use in subsequent reactions.

2.3. Synthesis of PdNPs@-β-CD-CMC

A 250 mL round-bottom flask was filled with 0.5 grams of β-CD-CMC and 50 mL of water, then stirred continuously for about 2 hours until a homogeneous solution was obtained. Subsequently, 5 mL of Pd(OAc)$_2$ solution in ethanol (30.0 mg mL^{-1}) was gradually added dropwise to the gel solution. Afterward, 20 μL of 1 M NaOH was introduced, and the mixture was sonicated for 2 hours. The resulting yellow solution was heated under microwave conditions (100 °C, 800 W) for 5 minutes, leading to the formation of a black solution, indicating the successful reduction of Pd^{2+} ions to PdNPs. The PdNPs@β-CD-CMC nanocomposites were then isolated and purified *via* centrifugation (12 000 rpm, 4 °C, 30 minutes). The resulting nanocomposite powder was then dried at 60 °C for 12 hours and kept at room temperature for future use.[41]

2.4. Physicochemical characterization of PdNPs@-β-CD-CMC

A JASCO V-630 spectrophotometer was utilized to perform UV-vis spectroscopy (USA) over the wavelength range of 200–800 nm. FTIR and Raman spectra of β-CD, CMC, the gel systems (β-CD-CMC), Pd(OAc)$_2$, and PdNPs@β-CD-CMC were obtained using a Bruker Tensor 27 FTIR spectrometer (Germany) and an Xplora Plus Raman spectrometer (Horiba, France), respectively. The crystal structure of PdNPs was analyzed using X-ray diffraction (XRD) with a Bruker D8 Advance diffractometer.

The nanocomposite's particle size and zeta potential in aqueous solution were determined at 25 °C using a NanoPartica Horiba SZ-100 particle analyzer (Japan). Elemental composition and distribution were analyzed *via* energy-dispersive X-ray spectroscopy (EDX) using a Horiba EMAX ENERGY EX-400 system. Thermogravimetric analysis (TGA) was performed on a LabSys evo S60/58988 thermoanalyzer (Setaram, France) from 30 °C to 800 °C, with a heating rate of 10 °C min^{-1} under an air atmosphere.

^{1}H (600 MHz) and ^{13}C (150 MHz) nuclear magnetic resonance (NMR) spectra were recorded using a Bruker Advance 600 spectrometer, employing CDCl$_3$ as the solvent and tetramethylsilane (TMS) as the internal reference. Gas chromatography (GC) analysis was conducted on a Shimadzu GCMS-QP2020 system (Japan) fitted with an Rxi-5MS capillary column (30 m in length, 0.25 mm in inner diameter, and 0.25 μm in film thickness, Shimadzu, Japan).

2.5. Catalytic activity for Sonogashira coupling

A sealed reaction container was loaded with phenylacetylene **1a** (50 mg, 0.49 mmol, 53 μL, 1.0 equiv.), iodobenzene **2c** (100 mg, 0.49 mmol, 55 μL), CuI (1.0 mol%, 1.9 mg, 0.0098 mmol), PPh$_3$ (6.0 mol%, 7.70 mg, 0.0294 mmol), K$_2$CO$_3$ (70 mg, 0.49 mmol, 1.0 equiv.), and PdNPs@β-CD-CMC (10 mg) in 1.0 mL of anhydrous DMF. The reaction mixture was maintained at a temperature of 130 °C in an oil bath for 3 hours. Once cooled to room temperature, DMF was removed under vacuum conditions. The unrefined product was subsequently purified through silica gel column chromatography (230–400 mesh) using a gradient elution with *n*-hexane, resulting in compound **3a** as a purified product with a 96% yield (Table 2).

2.5.1 1,2-Diphenylethyne (3a). White solid; yield 96%; R_f = 0.7 (*n*-hexane); mp = 62–64 °C; ^{1}H NMR (600 MHz, CDCl$_3$): δ 7.54–7.52 (m, 4H), 7.55–7.32 (m, 6H); ^{13}C NMR (150 MHz, CDCl$_3$): δ 131.6, 128.4, 128.3, 123.3, and 89.4 ppm.

2.5.2 1-Methyl-4-(phenylethynyl)benzene (3b). White solid; yield 94%; R_f = 0.6 (*n*-hexane); mp = 75–77 °C; ^{1}H NMR (600 MHz, CDCl$_3$): δ 7.64–7.61 (m, 2H), 7.38–7.36 (m, 2H), 7.35–7.34 (m, 3H), 7.18–7.16 (m, 2H), 2.38 (s, 3H); ^{13}C NMR (150 MHz, CDCl$_3$): δ 138.3, 131.6, 131.1, 129.6, 129.1, 128.4, 123.0, 120.7, 89.4, 88.9, and 21.5 ppm.

2.5.3 1-Methoxy-4-(phenylethynyl)benzene (3c). White solid; yield 95%; R_f = 0.4 (*n*-hexane); mp = 97–99 °C; ^{1}H NMR (600 MHz, CDCl$_3$): δ 7.52–7.46 (m, 4H), 7.34–7.30 (m, 3H), 6.88 (d, *J* = 8.5 Hz, 2H), 3.83 (s, 3H); ^{13}C (150 MHz, CDCl$_3$): δ 159.6, 133.1, 131.5, 128.3, 127.9, 123.6, 115.4, 113.9, 89.4, 89.2, and 55.3 ppm.

2.5.4 1,2-Di-*p*-tolylethyne (3d). White solid; yield 95%; R_f = 0.7 (*n*-hexane); mp = 118–120 °C; ^{1}H NMR (600 MHz, CDCl$_3$); ^{1}H NMR (600 MHz, CDCl$_3$): δ 7.54–7.52 (m, 2H), 7.49 (d, *J* = 7.5 Hz, 1H), 7.35–7.31 (m, 3H), 7.22 (d, *J* = 4.0 Hz, 2H), 7.17–7.14 (m, 1H), 2.51 (s, 3H); ^{13}C (150 MHz, CDCl$_3$): δ 140.2, 131.9, 131.6, 129.5, 128.5, 128.4, 128.2, 125.6, 123.6, 123.1, 93.4, 88.9, and 21.5 ppm.

2.5.5 4-(Phenylethynyl)benzonitrile (3e). White solid; yield 96%; R_f = 0.4 (*n*-hexane/ethyl acetate 5%); mp = 105–107 °C. ^{1}H NMR (600 MHz, CDCl$_3$): δ 7.66–7.69 (m, 4H), 7.56 (t, *J* = 4.8 Hz,

2H), 7.39–7.40 (m, 3H). ^{13}C NMR (150 MHz, CDCl$_3$): δ 131.6, 128.7, 128.4, 128.1, 123.3, 119.3, 87.0, 82.4, 24.7, 18.6, and 16.2 ppm.

2.5.6   1-Methoxy-3-(phenylethynyl)benzene (3f). White solid; yield 94%; R_f = 0.4 (n-hexane); mp = 74–75 °C. ^{1}H NMR (600 MHz, CDCl$_3$): δ 7.54–7.52 (m, 2H), 7.35–7.32 (m, 3H), 7.26–7.23 (m, 1H), 7.14–7.12 (m, 1H), 7.06 (dd, J = 3.6 Hz, 1H), 6.90–6.88 (m, 1H), 3.81 (s, 3H). ^{13}C NMR (150 MHz, CDCl$_3$): δ 159.4, 133.7, 129.4, 128.4, 128.3, 124.3, 124.2, 123.2, 116.4, 114.9, 89.3, 89.2 and 55.3 ppm.

2.5.7   1-Nitro-4-(phenylethynyl)benzene (3g). Yellow solid; yield 94%; R_f = 0.5 (n-hexane); mp = 110–112 °C. ^{1}H NMR (600 MHz, CDCl$_3$): δ 8.23–8.21 (m, 2H), 7.68–7.66 (m, 2H), 7.57–7.55 (m, 2H), 7.40–7.39 (m, 3H). ^{13}C NMR (150 MHz, CDCl$_3$): δ 132.1, 132.0, 130.6, 129.2, 128.7, 128.3, 122.2, 118.6, 111.5, 94.0 and 87.7 ppm.

2.6.   Catalytic activity for reduction of alkynes

In a Pyrex ground-bottom reaction flask, 1.5 mL of anhydrous DMF was degassed under a nitrogen atmosphere before adding KOH (1.5 mmol, 0.084 g), alkyne (**4**) (0.85 mmol), and PdNPs@β-CD-CMC catalyst (10 mg). The reaction mixture was continuously stirred and heated to 145 °C in an oil bath for 6 hours to achieve complete conversion. Once the reaction concluded, the mixture was allowed to cool to room temperature and extracted twice with n-hexane (2 × 25 mL). The organic layer was then thoroughly washed with water and dried over anhydrous MgSO$_4$. The solvent was evaporated under reduced pressure, yielding the crude product through filtration. Final purification was carried out using column chromatography with a n-hexane/diethyl ether mixture (9 : 1, v/v) as the eluent, resulting in the isolation of (Z)-alkenes (**5**) (Table 4).

2.6.1   Styrene (5a). GC-MS (m/z): 38, 51, 63, 78, 103, 104 (100). ^{1}H NMR (600 MHz, CDCl$_3$): δ 7.39–7.37 (m, 2H), 7.29 (dd, J = 15.6 Hz, 2H), 7.24–7.21 (m, 1H), 6.70 (dd, J = 28.8 Hz, 1H), 5.73 (dd, J = 18.6 Hz, 1H), 5.22 (dd, J = 10.8 Hz, 1H).

2.6.2   p-Methoxystyrene (5b). GC-MS (m/z): 15, 27, 39, 51, 65, 91, 119, 134 (100). ^{1}H NMR (600 MHz, CDCl$_3$): δ 7.34–7.31 (m, 2H), 6.85–6.83 (m, 2H), 6.65 (dd, J = 28.2 Hz, 1H), 5.59 (dd, J = 18.6 Hz, 1H), 5.11 (dd, J = 11.4 Hz, 1H), 3.77 (s, 3H).

2.6.3   cis-Stilbene (5c). GC-MS (m/z): 51, 76, 89, 102, 152, 165, 176, 180 (100). ^{1}H NMR (600 MHz, CDCl$_3$): δ 7.25–7.21 (m, 8H), 7.20–7.18 (m, 2H), 6.60 (s, 2H).

2.6.4   (Z)-2-(hex-3-en-1-yloxy)tetrahydro-2H-pyran (5d). GC-MS (m/z): 27, 41, 57, 67, 85 (100), 101. ^{1}H NMR (600 MHz, CDCl$_3$): δ 5.47–5.44 (m, 1H), 5.38–5.34 (m, 1H), 4.60 (dd, J = 7.2 Hz, 1H), 3.90–3.86 (m, 1H), 3.73 (dt, J = 24 Hz, 1H), 3.52–3.48 (m, 1H), 3.41 (dt, J = 14.4 Hz, 1H), 2.37–2.33 (m, 2H), 2.09–2.04 (m, 2H), 1.86–1.80 (m, 1H), 1.74–1.67 (m, 1H), 1.61–1.50 (m, 4H), 0.97 (t, J = 15 Hz, 3H). ^{13}C NMR (150 MHz, CDCl$_3$): δ 133.6, 125.0, 98.8, 67.2, 62.3, 30.8, 27.9, 25.5, 20.6, 19.6 and 14.3 ppm.

2.6.5   (Z)-2-(oct-3-en-1-yloxy)tetrahydro-2H-pyran (5e). ^{1}H NMR (600 MHz, CDCl$_3$): δ 5.47–5.44 (m, 1H), 5.41–5.34 (m, 1H), 4.60 (dd, J = 7.2 Hz, 1H), 3.80–3.86 (m, 1H), 3.73 (dt, J = 24 Hz, 1H), 3.52–3.48 (m, 1H), 3.41 (dt, J = 23.4 Hz, 1H), 2.35 (qd, J = 23.4 Hz, 2H), 2.07–2.04 (m, 2H), 1.87–1.80 (m, 1H), 1.75–1.66 (m, 1H), 1.60–1.56 (m, 2H), 1.48–1.07 (m, 2H), 1.36–1.29 (m, 4H). 0.93–0.88 (m, 3H). ^{13}C NMR (150 MHz, CDCl$_3$): δ 132.0, 125.5, 98.8, 67.1, 62.3, 31.8, 30.7, 28.0, 27.0, 25.5, 19.6 and 13.95 ppm.

3.   Results and discussion

3.1.   Preparation of β-CD-CMC

β-CD-CMC was synthesized by dissolving CMC and β-CD in water at mass ratios of 1 : 1, 1 : 2, and 2 : 3 (w/w), followed by sonication until a uniform mixture was achieved. The preparation method was adapted from previous instructional materials.[45] The synthetic procedure revealed that when amount of CMC exceeded that of β-CD, the mixture became more difficult to dissolve, requiring prolonged sonication. A solution containing only CMC without β-CD resulted in poor homogeneity, whereas using β-CD alone led to rapid PdNPs formation, but particle aggregation occurred. The structure of CMC features a cellulose backbone made up of D-glucose molecules joined by β-1,4-glycosidic linkage. Carboxymethyl groups (–CH$_2$–COOH) are attached to specific hydroxyl groups of the glucopyranose units within the chain. This modification enhances its water solubility, allowing it to dissolve readily in water at both high and low temperatures, resulting in a viscous solution.[46] β-CD is a heptasaccharide derived from glucose with moderate solubility in water. Therefore, the appropriate combination of CMC and β-CD in the right ratio is essential to stabilize PdNPs effectively (Fig. 1).

The functional groups present in the β-CD-CMC gel were characterized using FTIR spectroscopy. Fig. 2 illustrates the FTIR spectra of β-CD, CMC, and β-CD-CMC within the wavenumber range of 500–4000 cm^{-1}. The spectrum displays
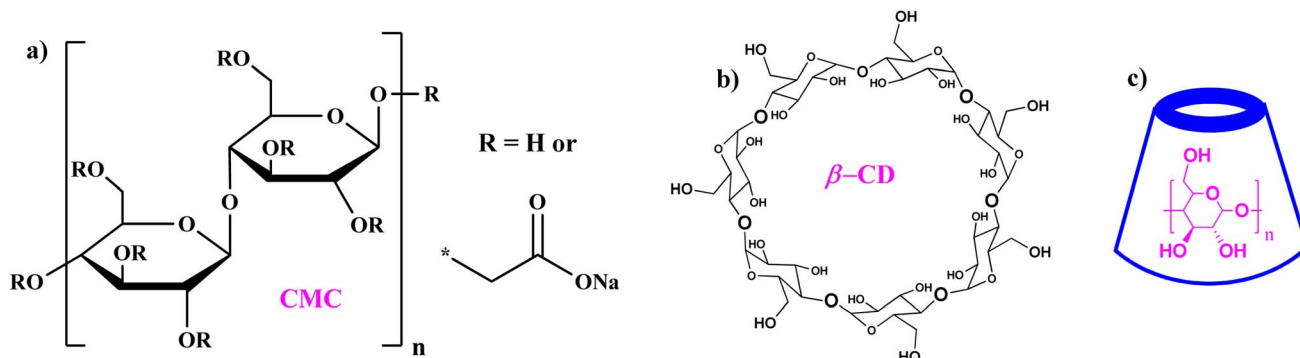
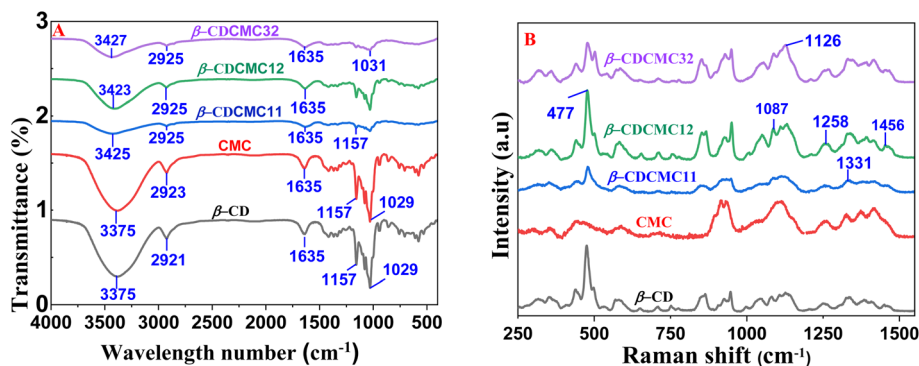**Fig. 1** Chemical structure (a) of CMC and shapes (b) and (c) of β-CD.

Fig. 2 (A) FT-IR spectra and (B) Raman spectra of β-CD-CMC.

characteristic absorption bands of both β-CD and CMC, exhibiting a wide peak at 3375 cm^{-1} associated with the O–H stretching vibration. Additionally, the asymmetric stretching vibration of C–H appears at 2921–2923 cm^{-1}, while the asymmetric stretching of C=O is observed at 1635 cm^{-1}. A peak at 1029 cm^{-1} is attributed to the C–O–C stretching vibration.[47–51] Notably, the FTIR spectra of the β-CD-CMC gel exhibit no substantial differences compared to the individual β-CD and CMC components, except for a shift in the O–H stretching band to a higher wavenumber (3423–3427 cm^{-1}), indicating possible intermolecular interactions in the gel system (Fig. 2A).

Raman spectra were obtained utilizing a 785 nm laser source, covering the wavenumber range of 200–3000 cm^{-1}. As illustrated in Fig. 3, spectra of the β-CD-CMC at various ratios exhibited characteristic vibrational bands, including a peak at 1456 cm^{-1} corresponding to C–H deformation, 1331 cm^{-1} associated with CH$_2$ deformation, and 1258 cm^{-1} attributed to in-plane O–H bending and CH$_2$ stretching. Additionally, a peak at 1126 cm^{-1} is attributed to symmetric C–O–C stretching, whereas the peaks at 1087 cm^{-1} are associated with both symmetric and asymmetric C–O–C stretching in glycosidic bonds. Additionally, a prominent band at 477 cm^{-1} is observed, representing skeletal vibrations of amylose (Fig. 2B).[52]

3.2. Preparation of PdNPs@-β-CD-CMC catalyst

The PdNPs@β-CD-CMC nanocomposite was synthesized following a previously reported method.[51] β-CD and CMC, serve as dual-function agents, acting as a reducer and a stabilizer in the conversion of metal cations to metal nanostructures (MNPs).[44] In this process, a water-containing solution of Pd^{2+} ions was incorporated with CMC and β-CD, then subjected to heating under microwave treatment (Microwave Synthesizer-Discover 2.0, 100 °C, 800 W) for 5 minutes, resulting in the formation of black PdNPs (Fig. 3A). The successful synthesis of PdNPs was confirmed using UV-vis spectroscopy. While pure CMC and β-CD do not exhibit any significant absorption peaks, the Pd^{2+} gel solution displays a characteristic peak at 279 nm, corresponding to electron exchange transitions of Pd^{2+} ions (Fig. 3B). Upon heating using microwave irradiation (100 °C 800 W) for 5 minutes, this peak disappears, Showing the complete conversion of Pd^{2+} and the successful generation of PdNPs on the β-CD-CMC matrix. The obtained nanocomposite was systematically characterized using various physicochemical techniques and demonstrated excellent catalytic effectiveness in the Sonogashira bond-forming reaction along with the selective reduction of alkynes to (Z)-alkenes.

3.3. Physicochemical characterizations of catalyst

The stability and size distribution of PdNPs@β-CD-CMC nanocomposites in aqueous solution were evaluated using zeta potential and dynamic light scattering (DLS) analysis at 25 °C (Fig. 4A–C). The zeta potential measurements revealed highly negative values of −24.0 mV (PdNPs@11), − 54.6 mV (PdNPs@12), and −55.1 mV (PdNPs@32), indicating strong
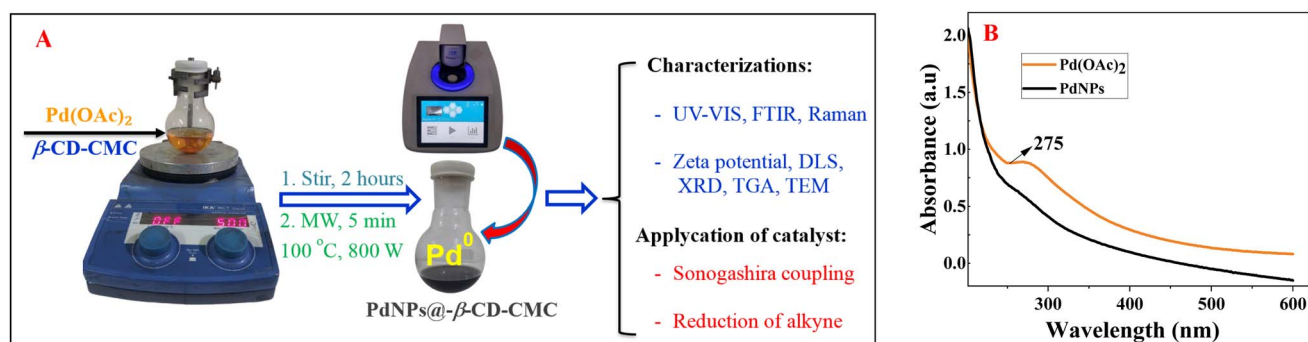

Fig. 3 (A) Diagrammatic depiction of the preparation of the catalyst and the application of PdNPs@-β-CD-CMC; and (B) UV-vis spectra of Pd(OAc)$_2$ and PdNPs@-β-CD-CMC.
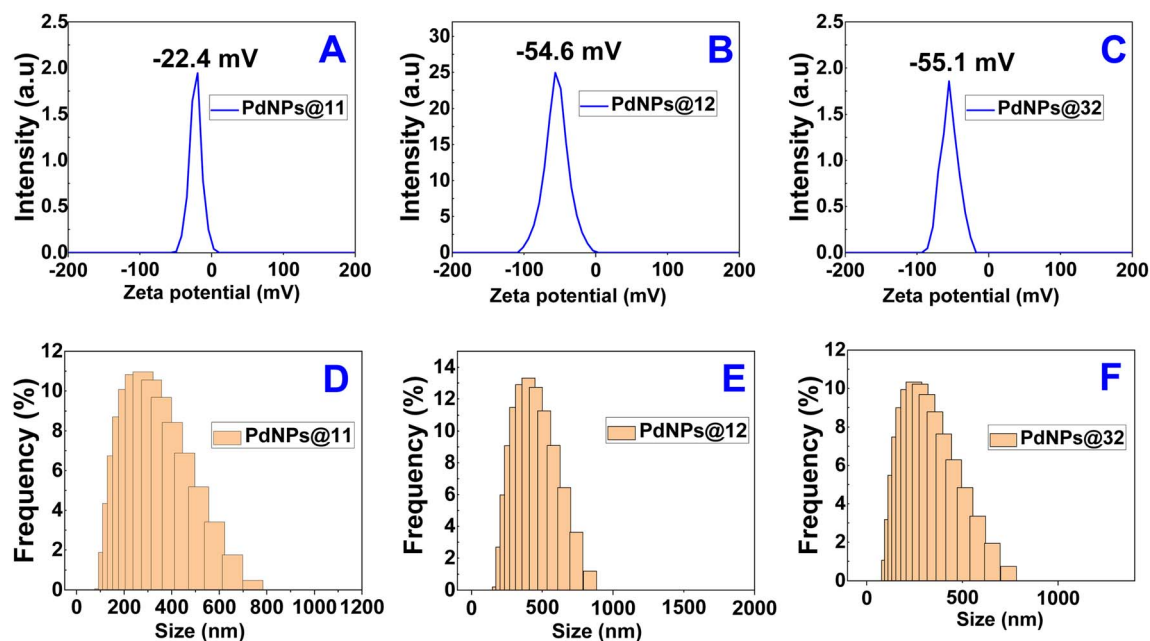
Fig. 4 Zeta potential (A–C) of PdNPs@β-CD-CMC; dynamic light scattering (D–F) of PdNPs@-β-CD-CMC.

electrostatic repulsion and excellent colloidal stability in solution. The DLS analysis further characterized the size distribution of the nanocomposites. The PdNPs@11 sample exhibited a monodisperse distribution with particle sizes ranging from 118 to 740 nm and an average hydrodynamic diameter of 293 nm (Fig. 4D). Similarly, PdNPs@12 displayed particle sizes between 193 and 837 nm, with an average particle diamete of 226 nm (Fig. 4E). Meanwhile, PdNPs@32 showed a size range of 118 to 740 nm, with an average hydrodynamic diameter of 285 nm (Fig. 4F). These results confirm that the polysaccharide chains of CMC and β-CD effectively stabilized the PdNPs, ensuring their dispersion and stability in aqueous media.[53]

The FTIR spectra of the PdNPs@β-CD-CMC catalyst were analyzed in comparison with those of its precursors, including Pd(OAc)$_2$, β-CD, and CMC, as illustrated in Fig. 7. The observed shifts or loss of distinctive peaks associated with Pd(OAc)$_2$ indicated the successful creation of Pd(0) nanoparticles. Markedly, the vibrational bands at 1602 cm^{-1} and 1332 cm^{-1} align with the irregular and regular stretching of the C=O bond, while a distinct peak at 1409 cm^{-1} is attributed to the carboxylate anion. The modifications in these oscillatory features after integrating Pd(OAc)$_2$ into the β-CD-CMC gel system confirm the conversion of Pd(II) ions. Furthermore, the absence of the characteristic Pd–O stretching peak at 691 cm^{-1} provides additional evidence for the formation of Pd(0) nanostructures. Moreover, the shift in the broad absorption band of –OH groups to 3433 cm^{-1} in the PdNPs@β-CD-CMC spectrum further supports the transformation of Pd(II) into Pd(0),
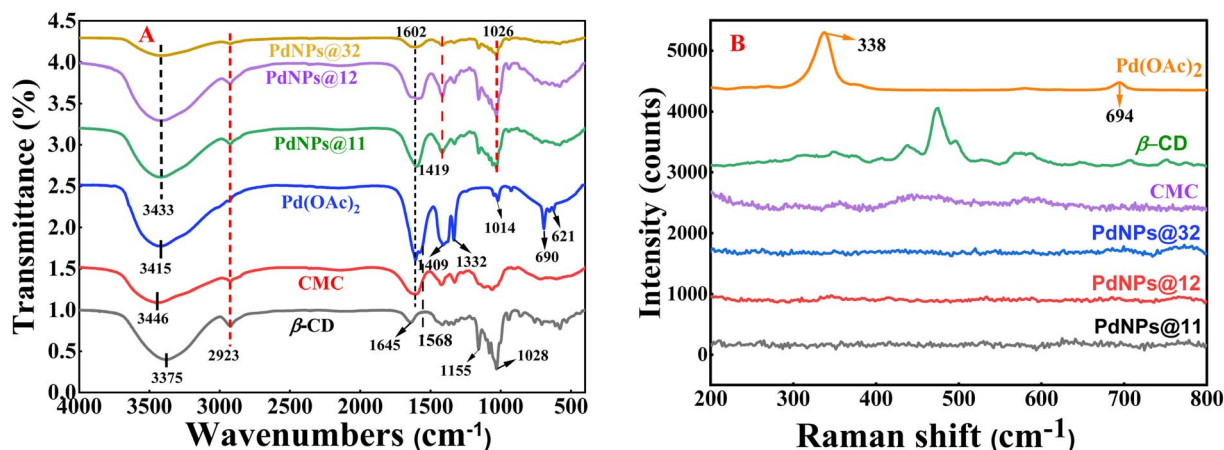

Fig. 5 (A) FT-IR spectra of PdNPs@-β-CD-CMC, Pd(OAc)$_2$, CMC and β-CD; and (B) Raman spectra of PdNPs@-β-CD-CMC, Pd(OAc)$_2$, CMC and β-CD.

facilitated by the occurrence of the β-CD-CMC gel system (Fig. 5A).[54–57]

Raman scattering spectroscopy was implemented to verify the establishment of PdNPs in the solid PdNPs@β-CD-CMC sample after separation. For comparison, the initial palladium precursors including Pd(OAc)$_2$, CMC and β-CD, were analyzed as reference materials. As illustrated in Fig. 5, the Raman spectrum of Pd(OAc)$_2$ exhibits distinct sharp and intense bands in the 800–200 cm^{-1} range, corresponding to the oscillatory patterns of the acetate ion and the C–O–Pd bond. A characteristic vibrational peak at 338 cm^{-1}, attributed to the Pd–O–C bond in Pd(OAc)$_2$, is observed alongside a weaker band at 694 cm^{-1} associated with the –CH$_3$ group (Fig. 5B). Notably, since Pd(0) lacks Raman activity,[58–60] the Raman spectra of PdNPs@β-CD-CMC do not display any significant peaks. The absence of these signals serves as compelling evidence for the accomplished formation of palladium nanomaterials within the β-CD-CMC gel matrix.

The structural properties of three PdNPs@β-CD-CMC catalysts were comprehensively analyzed using X-ray crystallography, which provided valuable insights into their crystallinity and confirmed the successful formation of PdNPs@β-CD-CMC nanostructures, as shown in Fig. 6A. The obtained diffraction pattern displayed distinct peaks at Bragg angles (2θ) of 40.1°, 46.3°, and 68.5°, relating to the (111), (200), and (220) crystal planes, respectively. These reflections are characteristic of the cubic crystal arrangement of metallic palladium with a face-centered configuration. Notably, the diffraction data revealed a strong preferential orientation along the (111) plane, as evidenced by its pronounced intensity. This preferential alignment suggests that a significant fraction of the palladium nanoparticles is oriented in this direction, which may influence their catalytic performance and structural stability.[53,60]

The thermal endurance of the PdNPs@-β-CD-CMC catalyst was assessed using thermogravimetric analysis (TGA) under an airflow of 20 mL per minute with a heating rate of 10 °C per minute (Fig. 6B). The thermal decomposition profiles of the three nanocomposite samples followed a similar trend, characterized by two distinct weight loss stages. At the initial stage (30–200 °C), PdNPs@32, PdNPs@12, and PdNPs@11 exhibited mass losses of 13%, 16%, and 18%, respectively, primarily due

to the vaporization of adsorbed water.[44] The following stage (200–600 °C) corresponded to further disintegration, with weight reductions of 68%, 65%, and 80%, respectively. Specifically, the degradation of polysaccharide components accounted for approximately 55%, 49%, and 62% of the total weight loss. The residual ash content in PdNPs@32, PdNPs@12, and PdNPs@11 was measured at 32%, 35%, and 20%, respectively, attributed to the presence of metallic palladium and carbonate residues. Notably, PdNPs@32 and PdNPs@12 retained 12–15% more ash than PdNPs@11, indicating a higher palladium content. Consequently, these nanocomposites were identified as promising candidates for catalytic applications in organic synthesis with reactions at high temperature.

The morphology and particle dimension of the nanocomposite were distinguished using TEM analysis. The TEM images verified the successful synthesis of the PdNPs@-β-CD-CMC catalyst, revealing spherical nanoparticles. Specifically, PdNPs@11 displayed a size distribution spanning from 2 to 10 nm, with a mean diameter of approximately 6.0–7.0 nm (Fig. 7A). Meanwhile, PdNPs@12 had particle sizes between 3.0 and 7.5 nm, meaning around 5.0–5.5 nm (Fig. 7B), and PdNPs@32 ranged from 2.5 to 6.0 nm, with an average size of 4–4.5 nm (Fig. 7C). The TEM images (Fig. 7) further confirmed that the PdNPs@-β-CD-CMC catalyst were uniformly dispersed within the β-CD-CMC gel matrix, with no signs of aggregation.

3.4. Catalytic performance for Sonogashira coupling reaction

A model coupling reaction between phenylacetylene derivatives and aryl halides (Ar–Cl, Ar–Br, and Ar–I) was designed for the PdNPs@-β-CD-CMC catalytic systems. The study systematically evaluated the impact of CuI co-catalyst, additives and the thermal condition on the reaction efficiency, with a summary of results provided in Table 1. To identify an optimal catalytic system, a mixture containing equal molar amounts of iodobenzene and phenylacetylene was heated in desiccated DMF under varying conditions. The reaction was performed using 10 mg of PdNPs@-β-CD-CMC, 6 mol% PPh$_3$, CuI, and one equivalent of base for 3 hours at 130 °C in a closed tube under a nitrogen atmosphere.
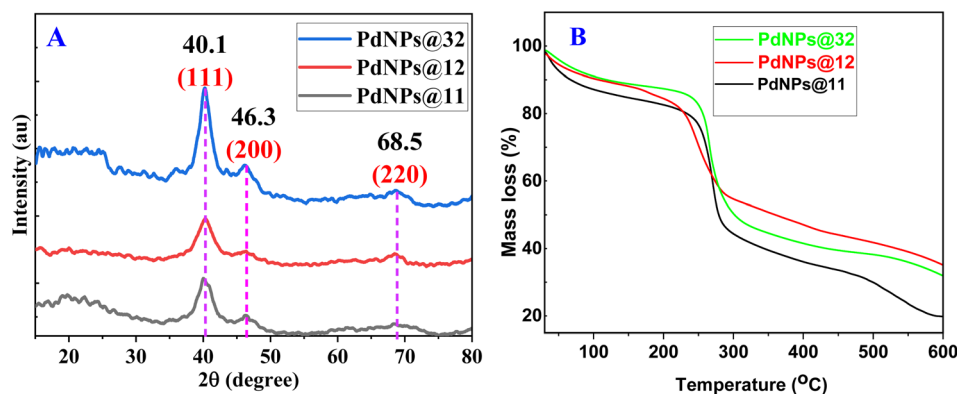

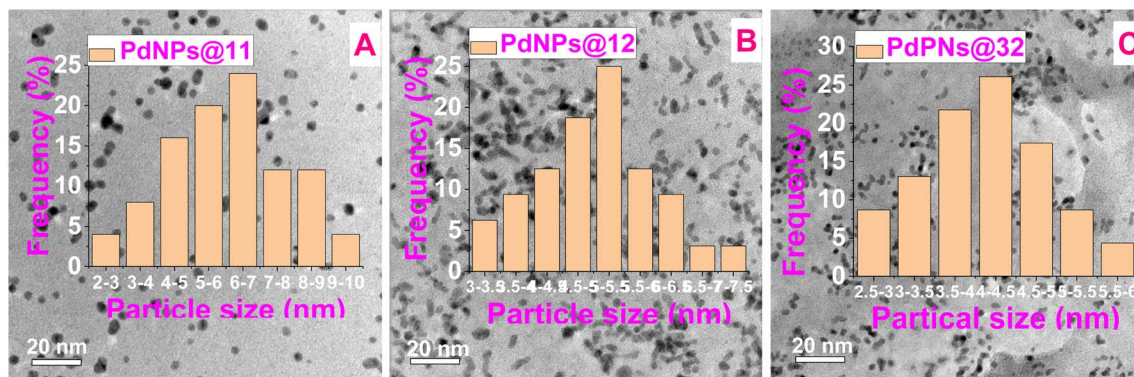Fig. 6 XRD pattern (A) and TGA curves (B) of PdNPs@-β-CD-CMC.

Fig. 7   TEM image of PdNPs@11, PdNPs@12, PdNPs@32.

The results indicated that the reaction occurred effectively at 90 °C in the company of both CuI and PdNPs@-β-CD-CMC, while also yielding good efficiencies at room temperature. However, analysis was complicated by the simultaneous formation of the product of the Sonogashira reaction and the Glaser coupling by product with the presence of CuI co-catalyst, both of which exhibited an identical R_f value (0.7) on TLC using n-hexane as the eluent. The presence of these products was further confirmed through ^{13}C NMR analysis.[61] To address this

issue, the reaction took place without the presence of CuI, using PdNPs@-β-CD-CMC along with an appropriate base, and PPh$_3$. Under these conditions, the reaction achieved a yield exceeding 89%. Previous studies have shown that the Sonogashira reaction can proceed efficiently under mild conditions, including aqueous environments, without CuI.[62–64] Notably, significant differences in synthetic yields were observed among the synthesized PdNPs catalysts. As shown in Table 1, PdNPs@12 and PdNPs@32 exhibited superior catalytic efficiency in the

Table 1   Reaction conditions for Sonogashira coupling catalyzed by PdNPs@-β-CD-CMC

Entry	[Cu] (mol%)	Base (equiv.)	Pd-catalyst (10 mg)	Temp. (°C)	Time (hours)	Yield^a (%)
1	CuI (10)	K$_2$CO$_3$	PdNPs@11	rt	3	23
2	CuI (10)	K$_2$CO$_3$	PdNPs@11	90	3	56
3	CuI (10)	K$_2$CO$_3$	PdNPs@11	130	3	63
4	CuI (10)	K$_2$CO$_3$	PdNPs@12	rt	3	34
5	CuI (10)	K$_2$CO$_3$	PdNPs@12	90	3	52
6	CuI (10)	K$_2$CO$_3$	PdNPs@12	130	3	67
7	CuI (10)	K$_2$CO$_3$	PdNPs@32	rt	3	30
8	CuI (10)	K$_2$CO$_3$	PdNPs@32	90	3	53
9	CuI (10)	K$_2$CO$_3$	PdNPs@32	130	3	58
10		K$_2$CO$_3$	PdNPs@11	rt	3	15
11		K$_2$CO$_3$	PdNPs@11	90	3	60
12		K$_2$CO$_3$	PdNPs@11	130	3	73
13		K$_2$CO$_3$	PdNPs@12	rt	3	16
14		K$_2$CO$_3$	PdNPs@12	90	3	78
15		K$_2$CO$_3$	PdNPs@12	130	3	90
16		K$_2$CO$_3$	PdNPs@32	rt	3	23
17		K$_2$CO$_3$	PdNPs@32	90	3	82
18		K$_2$CO$_3$	PdNPs@32	130	3	93
19		(Et)$_3$N	PdNPs@32	130	6	95
20	CuI (5)	K$_2$CO$_3$	PdNPs@12	130	6	67
21	CuI (5)	K$_2$CO$_3$	PdNPs@32	130	6	63
22	CuI (5)	(Et)$_3$N	PdNPs@12	130	6	64
23	CuI (5)	(Et)$_3$N	PdNPs@32	130	6	68

^{a} Yields were determined following purification via column chromatography on silica gel (SiO$_2$).

Table 2 1,2-Disubstituted alkynes synthesis using PdNPs@-β-CD-CMC catalyst under optimized reaction conditions

PdNPs@-β-CD-CMC-10 mg
1 mol-% CuI
→
1 eq. K$_2$CO$_3$, DMF, 6 mol-%PPh$_3$
130 °C, 3 hours

X: Cl, Br, I

Entry	Alkyne (1)	Aryl halide (2)	Product (3)	Time	Yield[a]	Entry	Alkyne (1)	Aryl halide (2)	Product (3)	Time	Isolated yield[a] (%)
1	1a	2a	3a	4	36	14	1b	2e	3d	5	95
2	1a	2b	3a	3	91	15	1a	2f	3e	4	54
3	1a	2c	3a	3	96	16	1a	2g	3e	3	89
4	1b	2a	3b	5	32	17	1a	2h	3e	3	96
5	1b	2b	3b	3	90	18	1a	2i	3f	4	89
6	1b	2c	3b	3	94	19	1a	2k	3f	3	94
7	1a	2d	3b	6	33	20	1a	2l	3g	4	70
8	1a	2e	3b	4	93	21	1a	2m	3g	4	87
9	1a	2f	3b	3	94	22	1a	2n	3g	3	94
10	1c	2a	3c	5	38	23	1a	2o	3c	5	40

Table 2 (*Contd.*)

R—X + ≡—R' → (PdNPs@-β-CD-CMC-10 mg, 1 mol-% CuI, 1 eq. K$_2$CO$_3$, DMF, 6 mol-%PPh$_3$, 130 °C, 3 hours) → R—≡—R'

X: Cl, Br, I

Entry	Alkyne (1)	Aryl halide (2)	Product (3)	Time	Yield[a]	Entry	Alkyne (1)	Aryl halide (2)	Product (3)	Time	Isolated yield[a] (%)
11	OCH$_3$ **1c**	Br **2b**	**3c** OCH$_3$	3	91	24	**1a**	Br OCH$_3$ **2p**	**3c** OCH$_3$	3	91
12	OCH$_3$ **1c**	I **2c**	**3c** OCH$_3$	3	95	25	**1a**	I OCH$_3$ **2q**	**3c** OCH$_3$	3	94
13	CH$_3$ **1b**	Br CH$_3$ **2d**	H$_3$C—≡—CH$_3$ **3d**	3	92						

[a] Yields were determined following purification *via* column chromatography on silica gel (SiO$_2$).

Sonogashira reaction compared to PdNPs@11 at 130 °C in the absence of CuI, with isolated yields exceeding 90% (entries 15 and 17). This enhanced performance is likely due to variations in the palladium content of the PdNPs@-β-CD-CMC catalyst. All purified products were identified through ^{1}H and ^{13}C NMR spectroscopy.

Furthermore, we explored the reactions of phenylacetylene coupling with various aryl halides. It is well established that activating the C–Cl bond is considerably more challenging than C–Br and C–I bonds.[65] When chlorobenzene was used as a substrate, the reaction proceeded with relatively low efficiency, yielding approximately 36% (Table 2, entry 1). However, the highly reactive 1-chloro-4-nitrobenzene exhibited significantly improved reactivity toward phenylacetylene, leading to higher yields (entries 15 and 20). In contrast, bromo- and iodo-substituted derivatives containing electron-providing groups, such as –CH$_3$ and –OCH$_3$, at the meta and para positions showed good reaction efficiency (Table 2, entries 8, 9, 13, 14, 18, 19, 24, 25). Additionally, the coupling of phenylacetylene derivatives bearing *para*-substituted –CH$_3$ and –OCH$_3$ groups resulted in promising yields (Table 2, entries 4–6, 10–12, 13–14).

In summary, PdNPs@12 and PdNPs@32 displayed superior catalytic activity in the Sonogashira coupling reaction. The coupling of diverse aryl halides with terminal alkynes proceeded efficiently without the necessity of CuI, highlighting the potential of PdNPs@12 and PdNPs@32 as effective catalysts for this transformation. Ongoing investigations are focused on extending the application of these catalysts to other types of coupling reactions, including the Heck, Suzuki, and Stille reactions.

Table 3 Reaction conditions for alkyne reaction in the presence of PdNPs@-β-CD-CMC

C$_4$H$_9$—≡—(CH$_2$)OTHP (**5a**) → (Pd-Catalyst-10 mg, Base/DMF, 145 °C) → C$_4$H$_9$ / (CH$_2$)OTHP, H, H (**5b**)

Entry	Base (equiv.)	Pd-catalyst (10 mg)	Temp.[a]	Time (hours)	Yield (%) (Z)-alkene
1	KOH	PdNPs@11	145	6	23
2	NaOH	PdNPs@11	145	6	56
3	KOH	PdNPs@11	145	8	63
4	KOH	PdNPs@12	145	6	34
5	NaOH	PdNPs@12	145	6	52
6	K$_2$CO$_3$	PdNPs@12	145	6	67
7	KOH	PdNPs@32	145	6	30
8	NaOH	PdNPs@32	145	6	53
9	KOH	PdNPs@11	145	6	64
10	KOH	PdNPs@12	145	6	86
11	KOH	PdNPs@32	145	6	95
12	KOH		145	12	0

[a] Temperature in oil.

3.5. Catalytic performance for reduction of alkynes

Table 3 presents the outcomes of the hydrogenation reaction of **5a**, facilitated by PdNPs@-β-CD-CMC catalysts, where DMF functions used as both the solvent and the hydrogen donor in varying conditions. In the case of a mixture containing **5a** and PdNPs@-β-CD-CMC (10 mg) in DMF was heated at 145 °C in an oil bath for around 6 hours under an inert atmosphere, the isolated yield of **5a** surpassed 95%. To evaluate the catalytic efficiency in alkyne transformations, we examined three catalyst systems: PdNPs@11, PdNPs@12, and PdNPs@32, employing 10 mg of catalyst along with one equivalent of base. The results indicated that PdNPs@12 and PdNPs@32 exhibited superior alkyne reduction performance compared to PdNPs@11. The selectivity toward (Z)-alkene was consistent with that achieved using Pd(OAc)$_2$, PdCl$_2$, Pd(PPh$_3$)$_2$Cl$_2$, Pd$_2$dba$_3$ and PdNPs@pectin as catalysts in previous reports.[31,44,66–68] Additionally, **5b** displayed high stereoselectivity, and it was successfully isolated with a yield exceeding 94% *via* column chromatography (entries 10 and 11).

As previous research has suggested that bases might promote DMF hydrolysis, we undertook experiments under the influence of K$_2$CO$_3$, NaOH, and KOH. The findings indicated that the addition of K$_2$CO$_3$ and NaOH almost had no impact among three PdNPs@-β-CD-CMC catalysts (Table 3), whereas introducing KOH significantly enhanced the partial hydrogenation of **5a**, leading to the formation of **5b** demonstrating superior stereoselectivity (entries 10 and 11). In the absence of PdNPs@-β-CD-CMC, the reaction did not proceed, even when the duration was extended by an additional 12 hours (entry 12).

In summary, PdNPs@12 and PdNPs@32 exhibited remarkable efficiency and chemoselectivity in converting alkynes to (Z)-alkenes, positioning them as promising catalysts for alkyne-to-(Z)-alkene transformations across various applications. The outstanding performance of these catalysts is likely ascribed to the palladium content in PdNPs@-β-CD-CMC.
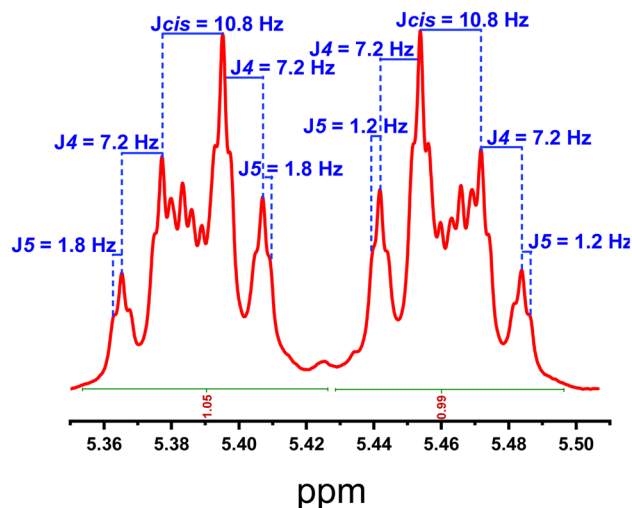

Fig. 8 The signals of the two protons at the double bond of compound **5e**.

Table 4 provides an overview of the semihydrogenation of diverse internal alkynes in DMF, using PdNPs@12 or PdNPs@32 (2 mol%) as catalysts in the involvement of KOH (1 equivalent) at 145 °C for about 6 hours. The reactions produced *cis*-alkenes with good to excellent yields and outstanding selectivity, similar to the performance of Pd(OAc)$_2$ reported in previous studies.[31] Notably, the hydrogenation of 3-butyn-1-ol (entry 8), 3-octyn-1-ol (entry 7) and 3-hexyn-1-ol (entry 6) failed to generate the corresponding *cis*-alkenes, even when the reaction duration was extended to 12 hours. However, introducing a tetrahydropyranyl (OTHP) protecting group to these alcohols significantly enhanced the reaction efficiency, yielding isolated products above 90% (entries 1–5). The reduced efficiency compared to the hydrogenation of aryl alkynes may be the consequence of the high volatility of alkyl alkenes. All purified products were analyzed using GC-MS and NMR (^{1}H and ^{13}C) spectroscopy.

To confirm that the synthesized product predominantly adopts the (Z)-alkene configuration, consistent with previously published reports,[31] we selected compound **5e** (entry 5) as a representative example. The ^{1}H NMR spectrum of **5e** exhibited signals corresponding to the two vinylic protons of the carbon chain, with chemical shifts at δ 5.34–5.41 ppm and 5.44–5.47 ppm. The coupling constants were observed as J_{cis} = 10.8 Hz, J_4 = 7.2 Hz, and J_5 = 1.2 Hz or 1.8 Hz. Given that the J_{cis} value of 10.8 Hz is less than 12 Hz when analyzing the proton signal splitting pattern, the structure of **5e** aligns with the predominant (Z)-alkene configuration (Fig. 8).

4. Conclusions

Conclusively, we explored a novel catalytic system, PdNPs@-β-CD-CMC, utilizing β-CD and CMC as reducing and stabilizing agents. The resulting nanocomposite featured palladium nanoparticles with an average dimension spanning 4 to 6 nm. Notably, the catalytic activity of PdNPs@12 and PdNPs@32 was

Table 4 Synthesis of (Z)-alkenes *via* optimized reaction conditions with PdNPs@-β-CD-CMC catalyst

$$R\!\!-\!\!\!\equiv\!\!\!-\!\!R' \xrightarrow[\text{DMF/KOH, 145 °C, 6h}]{\text{PdNPs@-β-CD-CMC-10 mg}} \begin{array}{c} H \quad\quad H \\ \diagdown\!\!=\!\!\diagup \\ R \quad\quad R' \end{array}$$

(4)   **(5)**

R, R': aryl, alkyl   *(Z)*-alkene

Entry	R	R′	Time (h)	Isolated yield[a] (%)
1	C$_6$H$_5$-	H	6	93 (**5a**)
2	*p*-CH$_3$O–C$_6$H$_5$-	H	6	95 (**5b**)
3	C$_6$H$_5$-	C$_6$H$_5$-	6	94 (**5c**)
4	C$_2$H$_5$-	-CH$_2$CH$_2$OTHP	6	93 (**5d**)
5	C$_4$H$_9$-	-CH$_2$CH$_2$OTHP	6	94 (**5e**)
6	C$_2$H$_5$-	-CH$_2$CH$_2$OH	12	Trace
7	C$_4$H$_9$-	-CH$_2$CH$_2$OH	12	Trace
8	H	-CH$_2$CH$_2$OH	10	Trace

[a] Yields were determined after purification through silica gel-based column chromatography (SiO$_2$).

appraised through the Sonogashira cross-coupling reaction and the reduction of alkynes. The high catalytic efficiency of the Sonogashira reaction for coupling in the absence of CuI at 130 °C was observed. The reaction between phenylacetylene and various aryl halide derivatives yielded excellent results when the halides were C–Br and C–I, while C–Cl exhibited lower efficiency unless the aromatic ring contained strongly electron-withdrawing groups. Most Sonogashira coupling reactions using the PdNPs@12 and PdNPs@32 catalytic system achieved an isolated yield of over 90%. The reduction of alkynes to (Z)-alkenes proceeded efficiently for both aromatic and aliphatic terminal alkynes, achieving an isolated yield of over 90%, with the (Z)-alkene configuration being predominant in terms of chemoselectivity. However, the PdNPs@32 catalytic system was recommended to use in the further study because its efficiency remains superior to that of the PdNPs@12 catalytic system. Therefore, PdNPs@32 catalytic system demonstrates significant potential for broad applications in various fields of organic synthesis.

Data availability

The data supporting this article have been included as part of the ESI.†

Author contributions

Van-Dung Le: conceptualization, funding acquisition, methodology, project administration, resources, supervision, validation, and writing – review & editing; T. Kim Chi Huynh, Van Nam Dao, Chi-Hien Dang, and Thi Yen Nghi Le: data curation, formal analysis, methodology, validation, visualization, and writing – review & editing.

Conflicts of interest

No potential conflict of interest was reported by the authors.

Acknowledgements

References

1 A. M. Trzeciak and A. W. Augustyniak, The role of palladium nanoparticles in catalytic C–C cross-coupling reactions, *Coord. Chem. Rev.*, 2019, **384**, 1–20.

2 A. Bej, K. Ghosh, A. Sarkar and D. W. Knight, Palladium nanoparticles in the catalysis of coupling reactions, *RSC Adv.*, 2016, **6**, 11446–11453.

3 D. Srimani, S. Sawoo and A. Sarkar, Convenient Synthesis of Palladium Nanoparticles and Catalysis of Hiyama Coupling Reaction in Water, *Org. Lett.*, 2007, **9**, 3639–3642.

4 B. Cornelio, G. A. Rance, M. L. Cochard, A. Fontana, J. Sapi and A. N. Khlobystov, Palladium nanoparticles on carbon nanotubes as catalysts of cross-coupling reactions, *J. Mater. Chem. A*, 2013, **1**, 8737–8744.

5 S. Luo, Z. Zeng, G. Zeng, Z. Liu, R. Xiao, M. Chen, L. Tang, W. Tang, C. Lai, M. Cheng, B. Shao, Q. Liang, H. Wang and D. Jiang, Metal Organic Frameworks as Robust Host of Palladium Nanoparticles in Heterogeneous Catalysis: Synthesis, Application, and Prospect, *ACS Appl. Mater. Interfaces*, 2019, **11**, 32579–32598.

6 A. Balanta, C. Godard and C. Claver, Pdnanoparticles for C–C coupling reactions, *Chem. Soc. Rev.*, 2011, **40**, 4973–4985.

7 M. Eckhardt and G. C. Fu, The First Applications of Carbene Ligands in Cross-Couplings of Alkyl Electrophiles: Sonogashira Reactions of Unactivated Alkyl Bromides and Iodides, *J. Am. Chem. Soc.*, 2003, **125**, 13642–13643.

8 T.-D. Nguyen, T.-T. Vo, C.-H. Nguyen, V.-D. Doan and C.-H. Dang, Biogenic palladium nanoclusters supported on hybrid nanocomposite 2-hydroxypropyl-β-cyclodextrin/alginate as a recyclable catalyst in aqueous medium, *J. Mol. Liq.*, 2019, **276**, 927–935.

9 M. Martins, C. Mourato, S. Sanches, J. P. Noronha, M. T. B. Crespo and I. A. C. Pereira, Biogenic platinum and palladium nanoparticles as new catalysts for the removal of pharmaceutical compounds, *Water Res.*, 2017, **108**, 160–168.

10 C. P. Adams, K. A. Walker, S. O. Obare and K. M. Docherty, Size-Dependent Antimicrobial Effects of Novel Palladium Nanoparticles, *PLoS One*, 2014, **9**, e85981.

11 X. Chen and X.-Y. Zhou, A Convenient, Efficient, and Inexpensive Copper(I) Complex Catalyzed Sonogashira Cross-Coupling of o-Iodoanilines with Terminal Alkynes, *Synthesis*, 2023, **55**, 1213–1220.

12 I. Favier, D. Pla and M. Gómez, Palladium Nanoparticles in Polyols: Synthesis, Catalytic Couplings, and Hydrogenations, *Chem. Rev.*, 2020, **120**, 1146–1183.

13 M. Zhang, P. S. Lee, C. Allais, R. A. Singer and J. P. Morken, Desymmetrization of Vicinal Bis(boronic) Esters by Enantioselective Suzuki-Miyaura Cross-Coupling Reaction, *J. Am. Chem. Soc.*, 2023, **145**, 8308–8313.

14 D.-H. Lee, H. Qiu, M.-H. Cho, I.-M. Lee and M.-J. Jin, Efficient Sonogashira Coupling Reaction Catalyzed by Palladium(II) β-Oxoiminatophosphane Complexes under Mild Conditions, *Synlett*, 2008, 1657–1660.

15 J. L. Alterman and G. A. Kraus, A Convenient Procedure for Sonogashira Reactions Using Propyne, *Synthesis*, 2022, **54**, 655–657.

16 M. L. Kantam, P. Srinivas, J. Yadav, P. R. Likhar and S. Bhargava, Trifunctional *N,N,O*-terdentate amido/pyridyl carboxylate Pd(II) complexes were highly active and stable phosphine-free catalysts for Heck and room-temperature Suzuki reactions with high turnover numbers, *J. Org. Chem.*, 2009, **74**, 4882–4885.

17 B. Karimi and D. Enders, New N-Heterocyclic Carbene Palladium Complex/Ionic Liquid Matrix Immobilized on Silica: Application as Recoverable Catalyst for the Heck Reaction, *Org. Lett.*, 2006, **8**, 1237–1240.

18 S. P. H. Mee, V. Lee and J. E, Stille Coupling Made Easier – The Synergic Effect of Copper(I) Salts and the Fluoride Ion, *Angew. Chem., Int. Ed.*, 2004, **43**, 1132–1136.

19 J.-H. Li, Y. Liang, D.-P. Wang, W.-J. Liu, Y.-X. Xie and D.-L. Yin, Efficient Stille Cross-Coupling Reaction Catalyzed by the Pd(OAc)₂/Dabco Catalytic System, *J. Org. Chem.*, 2005, **70**, 2832–2834.

20 B. M. Trost and R. Braslau, A Convenient Chemoselective Semihydrogenation of Acetylenes Using Homogeneous Catalysis, *Tetrahedron Lett.*, 1989, **30**, 4657–4660.

21 K. C. K. Swamy, A. S. Reddy, K. Sandeep and A. Kalyani, Advances in chemoselective and/or stereoselective semihydrogenation of alkynes, *Tetrahedron Lett.*, 2018, **59**, 419–429.

22 S. Rao and K. R. Prabhu, Stereodivergent Alkyne Reduction by using Water as the Hydrogen Source, *Chem.–Eur. J.*, 2018, **24**, 13954–13962.

23 S. Furukawa and T. Komatsu, Selective Hydrogenation of Functionalized Alkynes to (*E*)-Alkenes, Using Ordered Alloys as Catalysts, *ACS Catal.*, 2016, **6**, 2121–2125.

24 B. M. Trost, Z. T. Ball and T. Jöge, A Chemoselective Reduction of Alkynes to (*E*)-Alkenes, *J. Am. Chem. Soc.*, 2002, **124**, 7922–7923.

25 K. Chernichenko, Á. Madarász, I. Pápai, M. Nieger, M. Leskelä and T. Repo, A frustrated-Lewis-pair approach to catalytic reduction of alkynes to *cis*-alkenes, *Nat. Chem.*, 2013, **5**, 718–723.

26 F. A. Westerhaus, R. V. Jagadeesh, G. Wienhöfer, M. M. Pohl, J. Radnik, A. E. Surkus, J. Rabeah, K. Junge, H. Junge, M. Nielsen, A. Brückner and M. Beller, Heterogenized cobalt oxide catalysts for nitroarene reduction by pyrolysis of molecularly defined complexes, *Nat. Chem.*, 2013, **5**, 537–543.

27 J. A. Delgado, O. Benkirane, C. Claver, D. Curulla-Ferré and C. Godard, Advances in the preparation of highly selective nanocatalysts for the semi-hydrogenation of alkynes using colloidal approaches, *Dalton Trans.*, 2017, **46**, 12381–12403.

28 R. Shen, T. Chen, Y. Zhao, R. Qiu, Y. Zhou, S. Yin, X. Wang, M. Goto and L. B. Han, Facile Regio- and Stereoselective Hydrometalation of Alkynes with a Combination of Carboxylic Acids and Group 10 Transition Metal Complexes: Selective Hydrogenation of Alkynes with Formic Acid, *J. Am. Chem. Soc.*, 2011, **133**, 17037–17044.

29 K. Li, R. Khan, X. Zhang, Y. Gao, Y. Zhou, H. Tan, J. Chen and B. Fan, Cobalt catalyzed stereodivergent semi-hydrogenation of alkynes using H₂O as the hydrogen source, *Chem. Commun.*, 2019, **55**, 5663–5666.

30 Q. Ge, J. Ran, L. Wu and T. Xu, Selective reduction of aromatic nitro compounds over recyclable hollow fiber membrane-supported Au nanoparticles, *J. Appl. Polym. Sci.*, 2015, **132**, 41268.

31 J. Li, R. Hua and T. Liu, Highly Chemo- and Stereoselective Palladium-Catalyzed Transfer Semihydrogenation of Internal Alkynes Affording *cis*-Alkenes, *J. Org. Chem.*, 2010, **75**, 2966–2970.

32 P. P. Mpungose, Z. P. Vundla, G. E. M. Maguire and H. B. Friedric, The Current Status of Heterogeneous Palladium Catalysed Sonogashira and Suzuki Cross-Coupling Reactions, *Molecules*, 2018, **23**, 1676.

33 L. Yu, Y. Huang, Z. Wei, Y. Ding, C. Su and Q. Xu, Sonogashira Reactions Catalyzed by Ultrasmall and Uniform Pd Nanoparticles Supported on Polyaniline, *J. Org. Chem.*, 2015, **80**, 8677–8683.

34 L. O. Nyangasi, D. M. Andala, C. O. Onindo, J. C. Ngila, B. C. E. Makhubela and E. M. Ngigi, Preparation and Characterization of Pd Modified TiO₂ Nanofiber Catalyst for Carbon–Carbon Coupling Sonogashira Reaction, *J. Nanomater.*, 2017, 8290892.

35 R. Mangaiyarkarasi, M. Priyanga, N. Santhiya and S. Umadevi, *In situ* preparation of palladium nanoparticles in ionic liquid crystal microemulsion and their application in Sonogashira reaction, *J. Mol. Liq.*, 2020, **310**, 113241.

36 G. Zhang, H. Zhou, J. Hu, M. Liu and Y. Kuang, Pd nanoparticles catalyzed ligand-free Sonogashira reaction in ionic liquid microemulsion, *Green Chem.*, 2009, **11**, 1428–1432.

37 V. Calo, A. Nacci, A. Monopoli, A. Fornaro, L. Sabbatini, N. Cioffi and N. Ditaranto, Sonogashira Reaction Catalyzed by Nanosized Palladium on Chitosan in Ionic Liquids, *Organometallics*, 2004, **23**, 5154–5158.

38 A. I. Ayad, C. B. Marín, E. Colaco, C. Lefevre, C. Méthivier, A. O. Driss, J. Landoulsi and E. Guénin, "Water soluble" palladium nanoparticle engineering for C–C coupling, reduction and cyclization catalysis, *Green Chem.*, 2019, **21**, 6646–6657.

39 F. Diler, H. Burhan, H. Genc, E. Kuyuldar, M. Zengin, K. Cellat and F. Sen, Efficient preparation and application of monodisperse palladium loaded graphene oxide as a reusable and effective heterogeneous catalyst for suzuki cross-coupling reaction, *J. Mol. Liq.*, 2020, **298**, 111967.

40 O. Yuliarti and R. M. B. Othman, Temperature dependence of acid and calcium-induced low-methoxyl CMC and β-CD gel extracted from *Cyclea barbata* Miers, *Food Hydrocoll.*, 2018, **81**, 300–311.

41 Y. Xiao, S. Wang, J. Liu, H. Zhang and Y. Xu, Copper(II) mediated C–H methylthiolation of 2-phenyl pyridines with dimethyl sulfoxide using an amino acid ligand, *Tetrahedron Lett.*, 2019, **60**(19), 1317–1320.

42 A. F. Fracasso, C. A. Perussello, D. Carpiné, C. L. D. O. Petkowicz and C. W. I. Haminiuk, Chemical modification of citrus CMC and β-CD: Structural, physical and rheologial implications, *Int. J. Biol. Macromol.*, 2018, **109**, 784–792.

43 C. Xue, K. Palaniappan, G. Arumugam, S. A. Hackney, J. Liu and H. Liu, Sonogashira reactions catalyzed by water-soluble, β-cyclodextrin-capped palladium nanoparticles, *Catal. Lett.*, 2007, **116**, 94–100.

44 V. D. Le, T. C. H. Le, V. T. Chau, T. N. D. Le, C. H. Dang, T. T. N. Vo, T. D. Nguyen and T. D. Nguyen, Palladium nanoparticles in situ synthesized on Cyclea barbata pectin as a heterogeneous catalyst for Heck coupling in water, the reduction of nitrophenols and alkynes, *New J Chem.*, 2021, **45**, 4746–4755.

45 A. A. Mekkaoui, H. Orf and K. Bejtka, Carboxymethyl cellulose nanocolloids anchored Pd(0) nanoparticles (CMC@Pd NPs): synthesis, characterization, and catalytic

application in transfer hydrogenation, *Environ. Sci. Pollut. Res.*, 2023, **30**, 81619–81634.

46 C. B. Hollabaugh, L. H. Burt and W. A. Peterson, Carboxymethylcellulose. Uses and Applications, *Ind. Eng. Chem.*, 1945, **37**(10), 943–947.

47 A. Abdulhameed, H. M. Mbuvi, E. O. Changamu and F. M. Maingi, Microwave synthesis of Carboxymethylcellulose (CMC) fromRice Husk, *J. Appl. Chem.*, 2019, **12**(12), 33–42.

48 J. Ning, X. Luo, F. Wang and S. Huang, Synergetic Sensing Effect of Sodium CarboxymethylCellulose and Bismuth on Cadmium Detection byDifferential Pulse Anodic Stripping Voltammetry, *Sensors*, 2019, **19**, 5482.

49 R. Xu, X. Lin, J. Xu and C. Lei, Controlling the water absorption and improving the high C-ratestability: a coated Li-ion battery separator using β-cyclodextrin as binder, *Ionics*, 2020, **26**, 3359–3365.

50 S. Mosivand and I. Kazeminezhad, Functionalization and characterization of electrocrystallized iron oxide nanoparticles in the presence of β-cyclodextrin, *CrystEngComm*, 2016, **18**, 417–426.

51 Z. Naderi, J. Azizian, E. Moniri and N. Farhadyar, Synthesis and Characterization of Carboxymethyl Cellulose/β-Cyclodextrin/Chitosan Hydrogels and Investigating the Efect of Magnetic Nanoparticles (Fe$_3$O$_4$) on a Novel Carrier for a Controlled Release of Methotrexate as Drug Delivery, *J. Inorg. Organomet. Polym. Mater.*, 2020, **30**, 1339–1351.

52 E. Martwong, S. Chuetor and J. Junthip, Adsorption of Cationic Contaminants by Cyclodextrin Nanosponges Cross-Linked with 1,2,3,4-Butanetetracarboxylic Acid and Poly(vinyl alcohol), *Polymers*, 2022, **14**, 342.

53 K. Walbrück, F. Kuellmer, S. Witzleben and K. Guenther, Synthesis and Characterization of PVP-Stabilized Palladium Nanoparticles by XRD, SAXS, SP-ICP-MS, and SEM, *J. Nanomater.*, 2019, **2019**, 4758108.

54 M. Sarmah, A. B. Neog and P. K. Boruah, Effect of Substrates on Catalytic Activity of Biogenic Palladium Nanoparticles in C–C Cross-Coupling Reactions, *ACS Omega*, 2019, **4**, 3329–3340.

55 A. Biffis, P. Centomo, A. D. Zotto and M. Zecca, Pd Metal Catalysts for Cross-Couplings and Related Reactions in the 21st Century: A Critical Review, *Chem. Rev.*, 2018, **118**, 2249–2295.

56 J. E. Camp, J. J. Dunsford, E. P. Cannons, W. J. Restorick, A. Gadzhieva, M. W. Fay and R. J. Smith, Glucose-Derived Palladium(0) Nanoparticles as in Situ-Formed Catalysts for Suzuki-Miyaura Cross-Coupling Reactions in Isopropanol, *ACS Sustain. Chem. Eng.*, 2013, **2**, 500–505.

57 A. R. Hajipour and F. Mohammadsaleh, Triazole-Functionalized Silica Supported Palladium(II) Complex: A Novel and Highly Active Heterogeneous Nano-catalyst for C–C Coupling Reactions in Aqueous Media, *Catal. Lett.*, 2018, **148**, 1035–1046.

58 A. Baylet, P. Marécot and D. Duprez, In situ Raman and in situ XRD analysis of PdO reduction and Pd° oxidation supported on γ-Al2O3 catalyst under different atmospheres, *Phys. Chem. Chem. Phys.*, 2011, **13**, 4607–4613.

59 J. Zakrzewska and P. Uznanski, Synthesis and characterization of bis(amine) palladium(II) carboxylate complexes as precursors of palladium nanoparticles, *Dalton Trans.*, 2021, **50**, 6933–6948.

60 A. JyothiKora and L. Rastogi, Green synthesis of palladium nanoparticles using gum ghatti (*Anogeissus latifolia*) and its application as an antioxidant and catalyst, *Arab. J. Chem.*, 2018, **11**, 1097–1106.

61 N. Mishra, A. S. Singh, A. K. Agrahari, S. K. Singh, M. Singh and V. K. Tiwari, Glycosyl Triazole Ligand for Temperature-Dependent Competitive Reactions of Cu-Catalyzed Sonogashira Coupling and Glaser Coupling, *J. Org. Chem.*, 2021, **86**, 17884–17895.

62 P. Li, L. Wang and H. Li, Application of recoverable nanosized palladium(0) catalyst in Sonogashira reaction, *Tetrahedron*, 2005, **61**, 8633–8640.

63 B. H. Lipshutz, D. W. Chung and B. Rich, Sonogashira Couplings of Aryl Bromides: Room Temperature, Water Only, No Copper, *Org. Lett.*, 2008, **10**, 3793–3796.

64 J. He, K. Yang, J. Zhao and S. Cao, A highly efficient Pd-catalyzed Sonogashira coupling of terminal alkynes with both unreactive electron-rich fluoroarenes and electron-poor fluoroarenes afforded the corresponding internal alkynes in good yields in the presence of LiHMDS, *Org. Lett.*, 2019, **21**, 9714–9718.

65 D. H. Lee, H. Qiu, M. H. Cho, I. M. Lee and M. J. Jin, Efficient Sonogashira Coupling Reaction Catalyzed by Palladium(II) b-Oxoiminatophosphane Complexes under Mild Conditions, *Synlett*, 2008, **11**, 1657–1660.

66 B. Liang, M. Dai, J. Chen and Z. Yang, Copper-Free Sonogashira Coupling Reaction with PdCl$_2$ in Water under Aerobic Conditions, *J. Org. Chem.*, 2005, **70**, 391–393.

67 A. Elangovan, Y. H. Wang and T. I. Ho, Sonogashira Coupling Reaction with Diminished Homocoupling, *Org. Lett.*, 2003, **5**, 1841–1844.

68 J. He, K. Yang, J. Zhao and S. Cao, A highly efficient Pd-catalyzed Sonogashira coupling of terminal alkynes with both unreactive electron-rich fluoroarenes and electron-poor fluoroarenes afforded the corresponding internal alkynes in good yields in the presence of LiHMDS, *Org. Lett.*, 2019, **21**, 9714–9718.